Available online at www.sciencedirect.com
SCIENCE DIRECT®
Journal of Sound and Vibration 287 (2005) 809–825
JOURNAL OF SOUND AND VIBRATION
www.elsevier.com/locate/jsvi

Experimental identification of linear oil-film coefficients using least-mean-square method in time domain

S.X. Zhao[a,*], H. Zhou[b], G. Meng[a], J. Zhu[b]

[a]*State Key Laboratory of Vibration, Shock and Noise, Shanghai Jiaotong University, 800 Dongchuan Road, Minhang District, Shanghai 200240, China*
[b]*Theory of Lubrication and Bearing Institute, Xi'an Jiaotong University, Xi'an 710049, China*

Received 13 January 2004; received in revised form 19 July 2004; accepted 15 December 2004
Available online 24 February 2005

Abstract

In general sense, under small perturbation the stability of rotor-bearing system can be determined by linear oil-film coefficients of hydrodynamic bearing and oil-film forces can also be expressed by these coefficients. This paper proposes an experimental method to identify these coefficients and presents their characteristics under various operational conditions. A delicate test rig is constructed and experimental data are acquired under various testing conditions. From the experimental data, the relative velocity of the journal and the oil-film forces can be obtained by using a differentiator. The coefficients are identified using least-mean-square method in time domain. Some identified results are compared with the theoretical data. The experimental results indicate that the linear oil-film dynamic coefficients are sensitive to the excitation amplitude. The intensity of sensitivity is varied for different coefficients. From the investigation, it can be concluded that the linear oil-film force model will be invalid once the condition of small perturbation is not satisfied.

1. Introduction

Journal bearings have been widely used in high-speed rotating machinery. Since dynamic characteristics of oil-film bearing affect the unbalance responses and stability of machines,

*Corresponding author. Fax: +86 21 54747451.
E-mail address: zhaosanxing@hotmail.com (S.X. Zhao).

0022-460X/$ - see front matter © 2005 Elsevier Ltd. All rights reserved.
doi:10.1016/j.jsv.2004.12.011

Nomenclature

c radial clearance, mm
$\mathbf{d}_1$ linear damping coefficient matrix
$d_{XX}, d_{XY}, d_{YX}, d_{YY}$ linear damping coefficients, N/m s^{-1}
$D_{XX}, D_{XY}, D_{YX}, D_{YY}$ dimensionless linear damping coefficients, $D_{i,j} = (d_{i,j}/\mu L)(c/R)^3$ $(i,j = X, Y)$
$f_1\, f_2, f_3$ concentrating forces, N
f_X, f_Y horizontal and vertical oil-film forces, N
$F = f\psi^2/\mu UL$ dimensionless force
$\mathbf{k}_1$ linear stiffness coefficient matrix
$k_{XX}, k_{XY}, k_{YX}, k_{YY}$ linear stiffness coefficients, N/m
$K_{XX}, K_{XY}, K_{YX}, K_{YY}$ dimensionless linear stiffness coefficients, $K_{i,j} = (k_{i,j}/\mu\omega L)(c/R)^3$ $(i,j = X, Y)$
L bearing length, mm
m mass of bearing housing (including bottom and top splints, four steel robs), kg
n effective size of data
R journal radius, mm
RV relative variation of the coefficients
U tangential surface velocity of the journal, m/s
x_1, y_1 journal's relative movement, mm
X, Y system coordinates, bearing housing's absolute movement
μ kinetic viscosity, Pa s
ω angular velocity of rotation shaft, rad/s
$\psi = 1.5‰$ relative clearance
δ dimensionless excitation amplitude
$(\cdot)$ d/dt, derivative with respect to time

Subscripts

X direction of X
Y direction of Y

obtaining reliable bearing oil-film coefficients becomes particularly important. However, there exist so many factors influencing on the dynamic characteristics of oil-film bearing (such as pressure boundary conditions, temperature boundary conditions, cavitations, etc.) that it is not easy to calculate oil-film coefficients accurately. Thus both experimental and theoretical investigations on oil-film coefficients of journal bearing are indispensable.

Since it is impossible to measure the linear oil-film coefficients directly, many experimental techniques have been developed to identify these bearing parameters. All of these techniques are featured by excitation of journal or rotor mass, measurement of the corresponding input force, and the associated response of the journal or rotor mass. An economical and convenient experimental method to estimate these dynamic coefficients is based on the impulse responses [1–4]. An impulse excitation covers a wide range of frequency characteristics, which increases the reliability of estimated coefficients. Tieu and Qiu proposed a method to determine the oil-film coefficients from two or more sets of unbalance responses [5]. They utilized the synchronous unbalance responses to simplify the calculation of coefficients. This method is convenient to estimate the coefficients of journal bearing on-line. Kostrzewsky and Flack used sinusoidal excitation to recognize oil-film coefficients [6,7]. Their method can produce high-energy and high signal-to-noise ratio responses in the specified frequency. This method has been widely applied in experimental studies, including this paper.

Notably, not so many successful studies on measuring bearing oil-film coefficients are available up to now. Agreement between experimental results and theoretical predictions has been observed only in some specific conditions. This paper is to identify the linear coefficients under various

operating conditions and study the influence of perturbation amplitude on these coefficients. The experimental study is performed on a deliberate test rig. The diameter of the test bearing is 152 mm. First, the relative velocity and oil-film forces of this bearing are obtained from the experimental data using a differentiating FIR filter. A least-mean-square method in time domain is then introduced, and eight linear oil-film dynamic coefficients are identified and evaluated. Detailed experimental procedures and data processing techniques are presented. Finally, some measurement results are compared with the theoretical data. The influence of excitation amplitude on these identified oil-film coefficients is also discussed.

2. Experimental techniques

2.1. Mathematical model

Based on the linear theory, the oil-film force increment of journal bearing is the linear algebraic function of displacements (x, y) and velocities $(\dot{x}, \dot{y})$ with respect to the journal's static equilibrium position (x_0, y_0), it can be written as

$$\begin{bmatrix} \Delta\tilde{f}_X \\ \Delta\tilde{f}_Y \end{bmatrix} = \mathbf{k}_1 \begin{bmatrix} x - x_0 \\ y - y_0 \end{bmatrix} + \mathbf{d}_1 \begin{bmatrix} \dot{x} \\ \dot{y} \end{bmatrix} = \begin{bmatrix} k_{XX} & k_{XY} \\ k_{YX} & k_{YY} \end{bmatrix} \begin{bmatrix} x - x_0 \\ y - y_0 \end{bmatrix} + \begin{bmatrix} d_{XX} & d_{XY} \\ d_{YX} & d_{YY} \end{bmatrix} \begin{bmatrix} \dot{x} \\ \dot{y} \end{bmatrix}, \quad (1)$$

where $\Delta\tilde{f}_X, \Delta\tilde{f}_Y$ are the oil-film force increments in the horizontal and vertical directions. $\mathbf{k}_1$ and $\mathbf{d}_1$ are the linear stiffness and damping coefficient matrices. They have their respective four linear coefficients. It is noted that once multi-sets of displacements (x, y), velocities $(\dot{x}, \dot{y})$ and oil-film force increments are obtained from the experiment, the linear oil-film coefficient matrices $\mathbf{k}_1$ and $\mathbf{d}_1$ can be identified.

2.2. Experiment setup

Fig. 1 shows a schematic diagram of the test rig. The test shaft (5) is supported by two identical five pad tilting-pad journal bearings (6) at both ends. A test bearing (13), diameter 152 mm, width 88.3 mm, radial clearance 0.114 mm, is mounted between the supports. The test bearing along with the bearing housing (11) and the metal gasket (16) sits on the bottom splint (17). The bottom splint is dragged by four steel rods (9) which are screwed on the top splint (12). The top splint is hung over the spring-opposed bellows (14) which sits on a stiff supporting framework (8). Using this suspension structure, the test bearing floats over the test shaft.

When high-pressured air makes the spring-opposed bellows expand, the top splint is pushed up. Consequently, the test bearing is dragged up. In this way, the equivalent static load, which can be controlled by the air pressure and measured by a pressure sensor (10), can be applied to the bearing. The static load can be up to 40 kN. In order to ensure the test bearing's parallel movement in the plane which is perpendicular to the axis of the shaft, eight smooth ground rollers (15) are employed. They are symmetrically located at both ends of the test bearing. These rollers prevent the test bearing from rotating, titling, and moving in the axial direction. Four smooth ground steel balls are put between bottom splint (17) and metal gasket (16) to minimize friction.

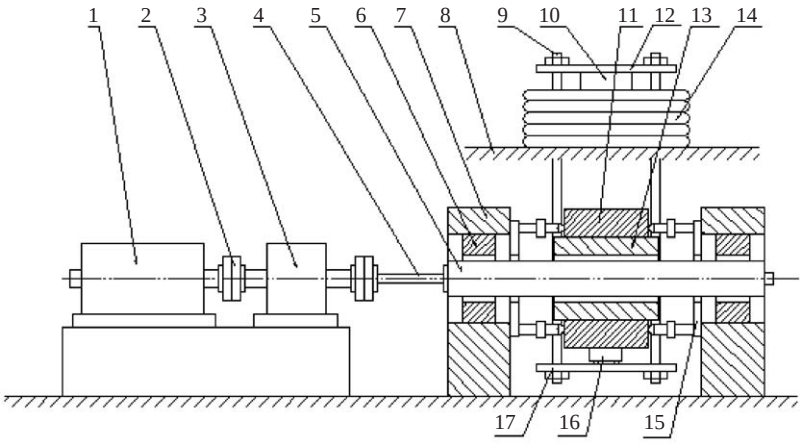

1) AC motor, 2) coupling, 3) gear box, 4) flexible bar coupling, 5) test shaft, 6) five pad tilting-pad journal bearing, 7) supporting bearing housing, 8) stiff supporting framework, 9) drag rod, 10) pressure sensor, 11) test bearing housing, 12) top splint, 13) test bearing, 14) spring-opposed bellows, 15) roller, 16) metal gasket, 17) bottom splint

Fig. 1. Outline of journal bearing test rig.

The shaft is driven by an 80 kW AC motor (1) through a gear box (3) and a flexible bar coupling (2). The rotational frequency can be adjusted by an infinitely variable transmission controller and can reach 60 Hz (3600 rev/min). The transmission ratio of the gear box is 2.8. Two separate oil supply systems are used to feed the lubricant into the gear box (3) and test bearing (13). The lubricant is turbine oil 22#, kinetic viscosity 48.65×10^{-3} Pa s at 20 °C and 28.25×10^{-3} Pa s at 30 °C.

It can be seen from Figs. 2 and 3 that two electric exciters compose the dynamic load system (Fig. 2-1). They are placed perpendicular to each other at 45° to the horizontal pointing to the geometric center of the test bearing. Each of the exciters is manipulated by an individual controller and driver system. The exciters can generate sinusoidal forces up to 1.5 kN in two directions simultaneously. And they are connected to the bearing housing by thin-walled tubular connecters. The pressure sensors (Fig. 2-2), which mount in the middle of connecters, are used to measure the excitation forces.

2.3. Oil-film force analysis

The oil-film forces in the experimental rig are analyzed in Fig. 4. Note that f_3 is the static load on the bearing, which is induced by pneumatic loading system; f_1 and f_2 are dynamic loads, which are generated by two exciters. In Fig. 4(a), the X and Y are absolute movement coordinates of the bearing housing. In Fig. 4(b), the x_1 and y_1 are relative movement coordinates of the rotor. The oil-film forces can be calculated from the following equations:

$$f_X = f_1 \cos 45^\circ - f_2 \cos 45^\circ + m\ddot{X},$$

$$f_Y = f_1 \sin 45^\circ + f_2 \sin 45^\circ + f_3 - mg + m\ddot{Y}, \quad (2)$$

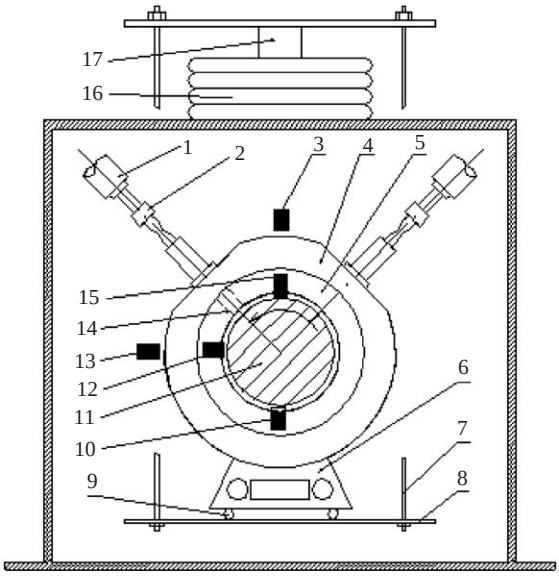

1) electric exciter, 2,17) pressure sensor, 3,12,13,15) eddy current sensor,
4) test bearing house, 5) test bearing, 6) metal gasket, 7) drag rod,
8) bottom splint, 9) steel ball, 10) temperature sensor, 11) test shaft,
14) oil inlet 16) spring-opposed bellows

Fig. 2. Outline of loading systems and sensors' locations.

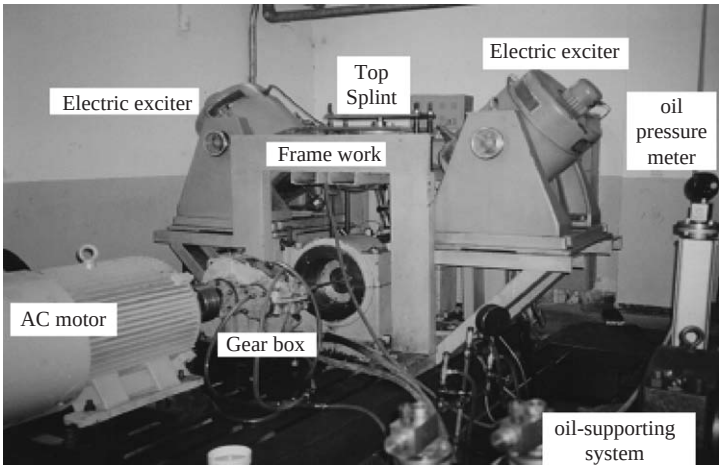

Fig. 3. Overview of the test rig.

where f_1, f_2, and f_3 can be measured from pressure sensors in the test rig. Each of f_1, f_2, f_3, f_X, and f_Y can be divided into two components: the static f_{i0} and the dynamic $\tilde{f}_i$ ($i = 1, 2, 3, X$, or Y). It should be pointed out that the static component of load f_3, i.e., f_{30}, is dominant, and the dynamic component $\tilde{f}_3$ which results from the pneumatic loading system is trivial. In the process of computing the dynamic oil-film force $\tilde{f}_Y$, the tiny dynamic component $\tilde{f}_3$ is taken into account.

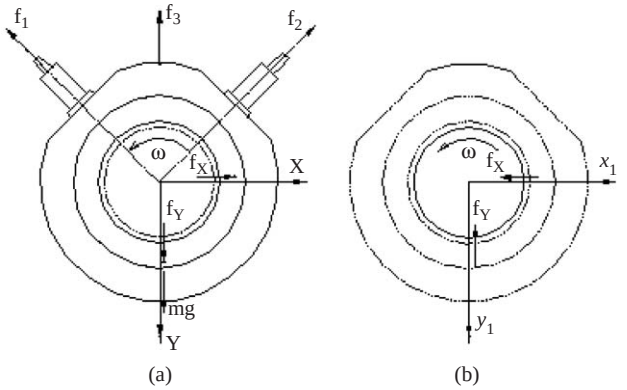

Fig. 4. Analysis of oil-film forces of bearing. (a) Forces acted on the bearing, (b) oil-film forces acted on the journal.

The detailed calculation procedure and data acquisition techniques are discussed in the next section.

2.4. Data acquisition

Displacement sensors and force sensors are employed to acquire testing data. The positions of these sensors are shown in Fig. 2. Six eddy current sensors (Tsinghua 8500) are used to measure displacements. Four of them (12 and 15) are installed on the test bearing housing at both ends of the test bearing to measure the relative displacements between the bearing and the journal in the horizontal and vertical directions (x_1, y_1). The other two (3 and 13) are installed on the framework to measure the absolute displacements of bearing housing in the horizontal and vertical directions (X, Y). A pressure sensor (17, GKCT15-1A) is positioned under the top splint to measure the pneumatic load (f_3). Another two pressure sensors (2, GKCT15-2C) are connected to the exciters to measure dynamic loads (f_1 and f_2). In addition, a temperature sensor (10) based on thermistor Pt is placed 0.5 mm under the surface of the bearing to determine the temperature data.

Each sensor is equipped with a separate amplifier and a highly accurate power supply to reach high accuracy in experiments. All signal cables are well shielded and grounded to avoid the electromagnetic disturbance from ambient devices. All amplifier outputs are regulated in the range of -10–10 V. Totally ten amplified channel-signals are connected to a data acquisition card (ADlink NuDAQ PCI-bus Card 9114). This data acquisition card is based on the 32-bit PCI Bus architecture with 16-bit precision and sampling rate up to 100 kHz. Fifty thousand data points per channel were captured at a rate of 5000 samples per second in the tests.

2.5. Experiment procedure

The experiments are executed in the following procedures:

1. Turn on the oil pump system; feed oil into the bearings and the gear box through two lubrication circuits.

2. Run AC motor and ensure the test shaft rotate at a given speed (300–1500 rev/s).
3. Start the air pressure system and increase the static load (f_3) to a given value (0–20 kN).
4. Turn on electric exciters and apply dynamic loads (f_1 and f_2) to the test bearing. (0–1.5 kN, sinusoidal wave 0–80 Hz).
5. When the system runs for about 5 min, the lubricant temperature becomes balanced and the working condition of journal bearing stays steady. Sample the testing data and transfer them to computer using the newly developed test application software.

Multi-sets of data have been obtained by repeating the aforementioned steps with different rotating speed, static load, dynamic loads, etc.

2.6. Data processing

Many sets of data are obtained in the experiments. A program based on Visual C++ 6.0 is newly developed to convert these data to standard ASCII files, which can be further processed by Matlab, Fortran and other popular software.

The velocity of the bearing can be calculated based on the displacement values through a designed differentiator (a FIR filter, see Appendix A). The differentiator can be reused to obtain accelerations ($\ddot{X}$, $\ddot{Y}$) from absolute velocities ($\dot{X}$, $\dot{Y}$) of bearing housing. Since the mass (m) of bearing housing is known in advance, the oil-film forces can be calculated using Eq. (2). Consequently, the oil-film forces, displacement and velocity in Eq. (1) are achieved. Next, the linear oil-film coefficients can be identified using the least-mean-square method.

Each set of data is processed as follows:

1. Feed the original data to a low-pass FIR filter to eliminate high-frequency noise.
2. Check the data of the eddy current sensor to find out whether they are in linear measurement range or not. Although the sensors are calibrated and installed carefully, their outputs may go beyond the linear measurement range in some cases. The displacements measured by eddy current sensor are the fundamental data in the following procedures. Accordingly, all of the data in this file are considered invalid if the output of an eddy current sensor is not in its own linear range.
3. Convert the data (voltage) from different channels into a corresponding physical value (displacement, force or temperature).
4. Due to the limitation of data acquisition card, input channels can only be sampled channel by channel instead of being sampled simultaneously. Consequently, there exist phase differences among channels. An interpolating FIR filter is designed to eliminate the phase differences. This filter serves the function as data interpolating, digital smoothing and data re-sampling. Using this filter, new groups of data can be re-constructed and the phase differences among channels can be eliminated.
5. Calculate the relative displacements (x_1, y_1) and absolute displacements (X, Y).
6. Calculate the velocity based on displacement values using the designed differentiator. After that, the acceleration ($\ddot{X}$, $\ddot{Y}$) can be achieved from the velocity ($\dot{X}$, $\dot{Y}$) by reusing the differentiator.

After the above procedures, a set of values about $(x_1, y_1, \dot{x}_1, \dot{y}_1, \ddot{X}, \ddot{Y}, f_1, f_2, f_3)$ can be obtained. Due to the FIR algorithm, the initial output data of a FIR filter is not available and should be discarded. The number of the discarded data equals to the number of the filter's tap. In order to ensure that the sizes of the above nine variables keep equal, the other data, which are not filtered, should be truncated correspondingly.

7. Compute the bearing oil-film forces using Eq. (2) and separate them into static parts (f_{X0}, f_{Y0}) and dynamic parts $(\tilde{f}_X, \tilde{f}_Y)$.
8. Recognize the linear oil-film coefficients using least-mean-square method.
9. Non-dimensionalize the coefficients.

3. Results and discussion

3.1. Coefficients identification

The oil-film force increment can also be written as

$$\Delta f_i(k) = k_{i,1}x_1(k) + k_{i,2}y_1(k) + k_{i,3}\dot{x}_1(k) + k_{i,4}\dot{y}_1(k) \quad (\text{for } i = X \text{ or } Y;\ k = 1-n), \tag{3}$$

where $\Delta f_i(k)$ is the oil-film force increment; n is the size of data obtained from each channel; $k_{i,1}$ and $k_{i,2}$ are linear stiffness coefficients; $k_{i,3}$ and $k_{i,4}$ are linear damping coefficients. It is assumed that $\tilde{f}_i(k)$ is the measured dynamic oil-film force (oil-film force increment) obtained from Eq. (2). The least-mean-square between $\Delta f_i(k)$ and $\tilde{f}_i(k)$ can be calculated as follows:

$$\min_{(\mathbf{k},\mathbf{d})} \varepsilon_i^2 = \sum_{k=1}^{n} [\Delta f_i(k) - \tilde{f}_i(k)]^2. \tag{4}$$

Then, the following equation is valid:

$$\frac{\partial \varepsilon_i^2}{\partial k_{i,p}} = 0 \quad (p = 1, \ldots, 4, \quad i = X, Y). \tag{5}$$

Combining Eqs. (3) and (5) yields:

$$\begin{bmatrix} \sum_{k=1}^{n} x_1(k)^2 & \sum_{k=1}^{n} x_1(k)y(k) & \sum_{k=1}^{n} x_1(k)\dot{x}_1(k) & \sum_{k=1}^{n} x_1(k)\dot{y}_1(k) \\ \sum_{k=1}^{n} y_1(k)x_1(k) & \sum_{k=1}^{n} y_1(k)^2 & \sum_{k=1}^{n} y_1(k)\dot{x}_1(k) & \sum_{k=1}^{n} y_1(k)\dot{y}_1(k) \\ \sum_{k=1}^{n} \dot{x}_1(k)x_1(k) & \sum_{k=1}^{n} \dot{x}_1(k)y_1(k) & \sum_{k=1}^{n} \dot{x}_1(k)^2 & \sum_{k=1}^{n} \dot{x}_1(k)\dot{y}_1(k) \\ \sum_{k=1}^{n} \dot{y}_1(k)x_1(k) & \sum_{k=1}^{n} \dot{y}_1(k)y_1(k) & \sum_{k=1}^{n} \dot{y}_1(k)\dot{x}_1(k) & \sum_{k=1}^{n} \dot{y}_1(k)^2 \end{bmatrix} \begin{bmatrix} k_{i,1} \\ k_{i,2} \\ k_{i,3} \\ k_{i,4} \end{bmatrix} = \begin{bmatrix} \sum_{k=1}^{n} x_1(k)\tilde{f}_i(k) \\ \sum_{k=1}^{n} y_1(k)\tilde{f}_i(k) \\ \sum_{k=1}^{n} \dot{x}_1(k)\tilde{f}_i(k) \\ \sum_{k=1}^{n} \dot{y}_1(k)\tilde{f}_i(k) \end{bmatrix}, \tag{6}$$

where $k_{X,1}, k_{X,2}, k_{Y,1}$, and $k_{Y,2}$ correspond to linear stiffness coefficients k_{XX}, k_{XY}, k_{YX}, and k_{YY} in Eq. (1); $k_{X,3}, k_{X,4}, k_{Y,3}$, and $k_{Y,4}$ correspond to linear damping coefficients $d_{XX}, d_{XY}, d_{YX}, d_{YY}$ in

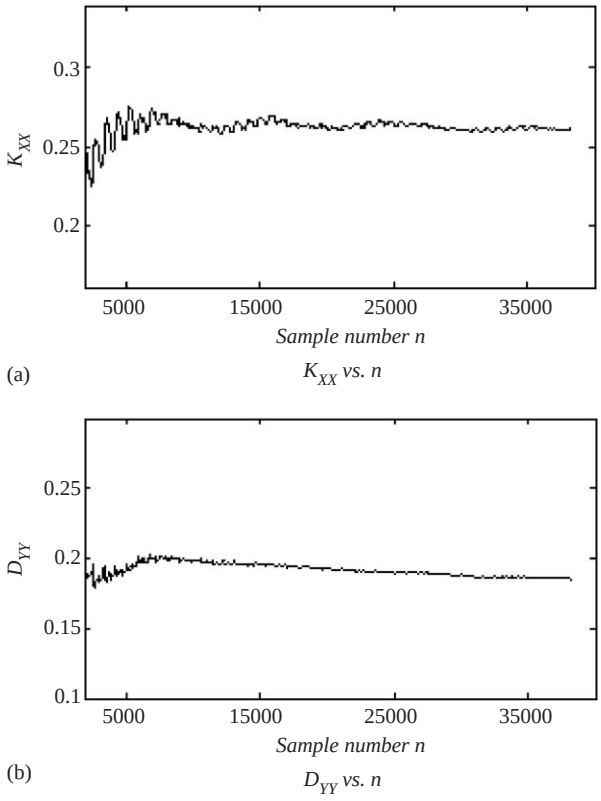

Fig. 5. Identified coefficients vs. sample number n.

Eq. (1). Accordingly, the eight linear oil-film dynamic coefficients can be rearranged into two sets $((k_{XX}, k_{XY}, d_{XX}, d_{XY})$ and $(k_{YX}, k_{YY}, d_{YX}, d_{YY}))$. They can be solved from two linear algebraic sets of equations. The two linear algebraic sets of equations have the same coefficient matrix, but with different vectors on the right-hand side. As the number of sample points increases, the coefficient matrix and right-hand vector gradually change. It can be seen from Fig. 5 that the identified coefficients will become steady when the number of sample points is big enough.

3.2. The effect of load parameter on linear coefficients

Under a given working condition, the load of bearing (f_{Y0}, the static load) can be calculated. A load parameter F_Y can be obtained as follows:

$$\frac{f_{Y0}}{F_Y} = \frac{\mu UL}{\psi^2}. \tag{7}$$

The load parameter F_Y is a comprehensive parameter in which bearing load, journal's rotating speed, lubricant temperature and viscosity of lubricant are involved. Therefore, the load

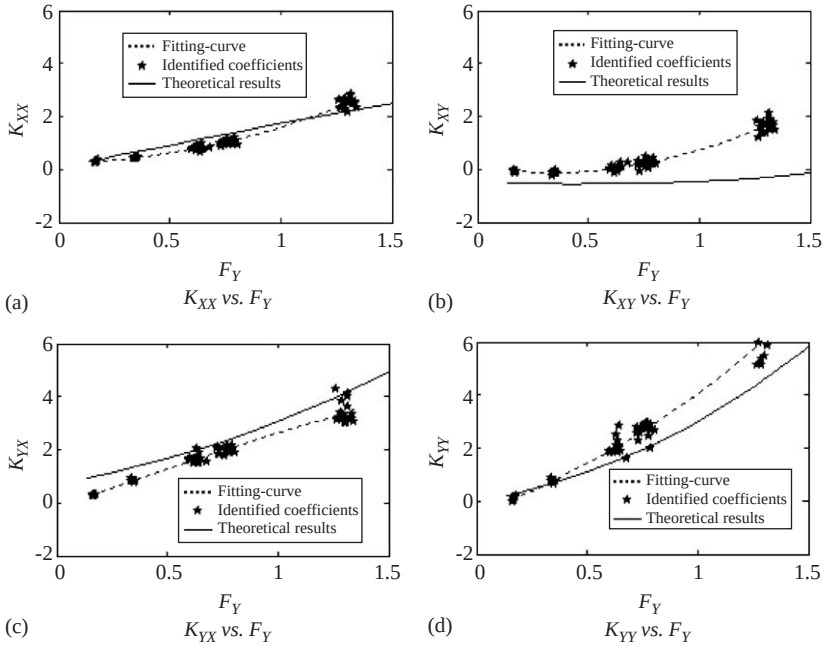

Fig. 6. Linear stiffness coefficients vs. load parameter F_Y.

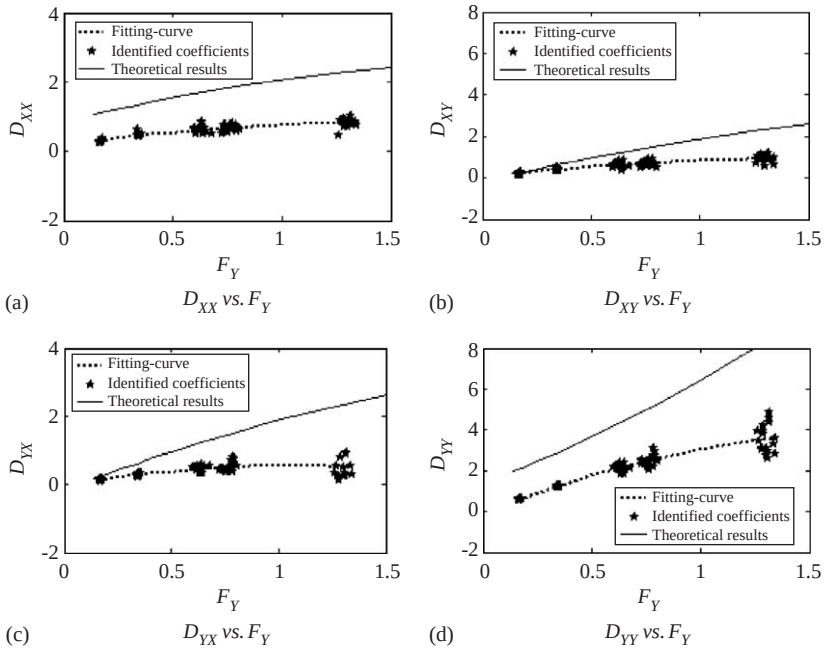

Fig. 7. Linear damping coefficients vs. load parameter F_Y.

parameter is suitable to characterize the operating condition of the bearing. Figs. 6 and 7 present the characteristics of linear stiffness and damping coefficients under various load parameters. There are 43 points, which are identified from 43 sets of testing data, in each figure. The dashed lines are the quadratic polynomial fitting curve of the identified coefficients. The solid lines represent the theoretical oil-film coefficients, which are calculated from the coupled generalized Reynolds and energy equations using finite element method [8]. The pressure boundary conditions are as follows:

$$p = p_0 \quad \text{at the grooves of bearing,}$$
$$p = 0 \quad \text{at the both ends of bearing.}$$

p_0 is the supply pressure, it can be determined by an oil-pressure meter.

As shown in Figs. 6 and 7, both the theoretical and experimental results show that the stiffness and damping coefficients increase with the growth of load parameter. The difference between them changes with the load parameter, and with coefficients. In general, the two results have similar trends, and the difference is smaller when the load parameters are small.

When F_Y is less than 0.5, most of identified results are close to the fitting curve. When F_Y is greater than 1, the results are scattered away from the fitting curve significantly. It turns out that the identified coefficients become less stable when F_Y increases, which indicates that nonlinear components of the oil-film forces have significant impact on the identified dynamic coefficients when F_Y becomes larger. Therefore, more attention should be paid for identifying the linear coefficients in the case of large load parameters.

Comparing the figures, it can be shown that less degree of scatter occurs in the stiffness coefficients than in the damping coefficients. The main reason for this phenomenon is that the velocity is obtained from the differentiator. The filter introduces some noise in the calculation, so the velocity error is larger than the displacement error. Additionally, the components of velocity have much more effect on damping coefficients than on stiffness coefficients.

An alternative method for obtaining less error velocity is based on the analytical expression of displacement [10].

3.3. The effect of excitation amplitude on the identified dynamic coefficients

Figs. 8 and 9 present the identified stiffness and damping coefficients at different excitation amplitude, under the condition of $F_Y = 0.35$. The x-axis indicates the maximum dimensionless excitation amplitude, which is defined as $\delta = LK/c$, where $LK = \max(\sqrt{x_1^2 + y_1^2})$, x_1 and y_1 are relative displacements of the bearing in two coordinates. c is the radial clearance of bearing. By this means, the value of excitation amplitude can be represented by δ.

In order to find out the relationship between each coefficient and δ, a cubic polynomial is constructed to fit the identified coefficients as

$$KD(\delta) = a_1\delta^3 + b_1\delta^2 + c_1\delta + d_1, \tag{8}$$

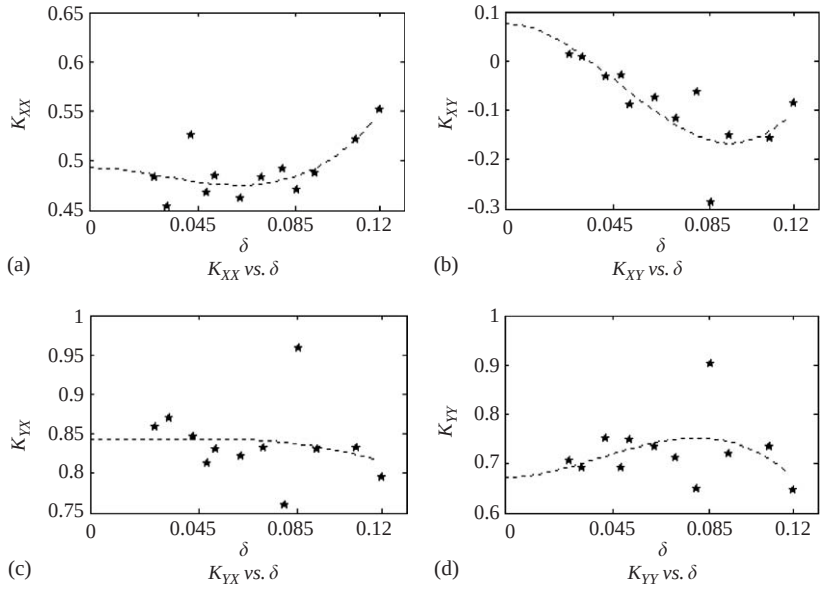

Fig. 8. Linear stiffness coefficients vs. dimensionless excitation amplitude δ ($F_Y = 0.35$).

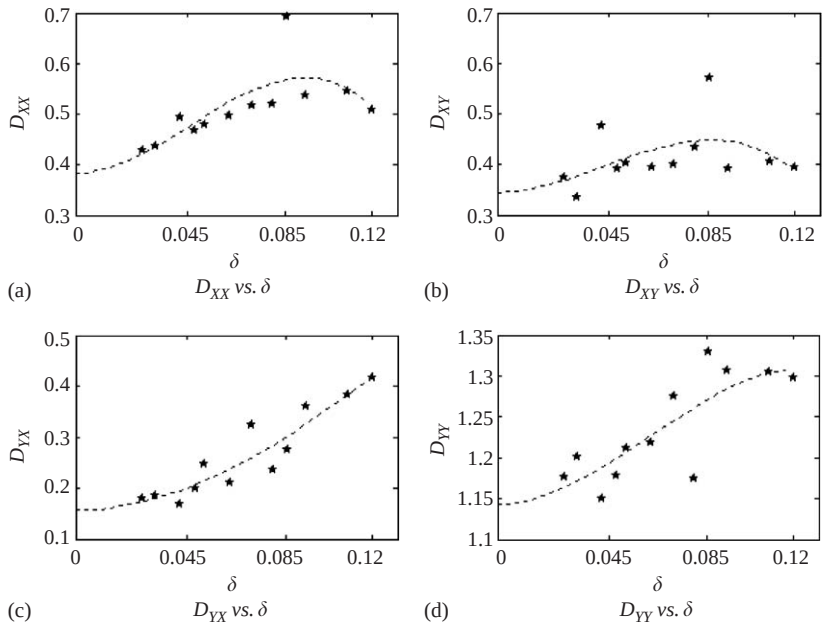

Fig. 9. Linear damping coefficients vs. dimensionless excitation amplitude δ ($F_Y = 0.35$).

where a_1, b_1, c_1 and d_1 are constants. When the perturbation acting on the bearing is sufficiently small, the linear coefficients should remain unchanged [9]. Therefore, each coefficient should be a constant when $\delta \to 0$. Accordingly, the following equation is valid:

$$\left.\frac{\partial KD}{\partial \delta}\right|_{\delta=0} = 0. \tag{9}$$

Combining Eqs. (8) and (9) yields $c_1 = 0$. Eq. (8) can be further rewritten as

$$KD(\delta) = a_1\delta^3 + b_1\delta^2 + d_1. \tag{10}$$

The least-mean-square method is also employed to determine the parameters a_1, b_1 and d_1. The dashed fitting curve in each figure is established by this method. The influence of excitation amplitude on these identified coefficients can be observed with the aid of these curves. However, it is difficult to evaluate the influence intensity of δ on different coefficients due to the different scales of each figure. A relative variation (RV) of the coefficient is introduced to solve this problem. It is defined as follows:

$$\mathrm{RV}(\delta) = \frac{KD(\delta) - KD(0)}{KD(0)}. \tag{11}$$

Eight RVs correspond to eight linear coefficients of bearing. The results are presented in Figs. 10 and 11.

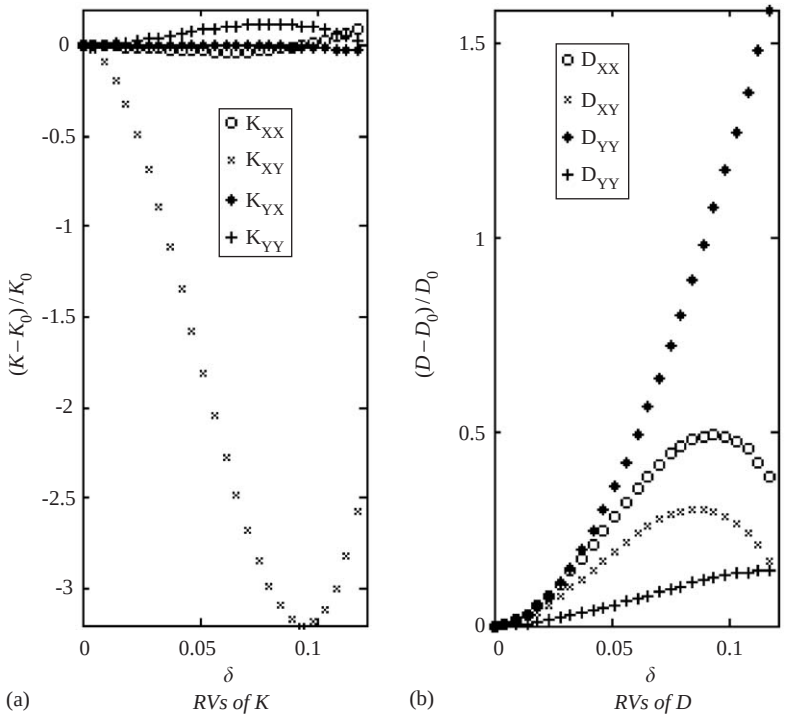

Fig. 10. Relative variations of linear coefficients of bearing vs. dimensionless excitation amplitude δ ($F_Y = 0.35$).

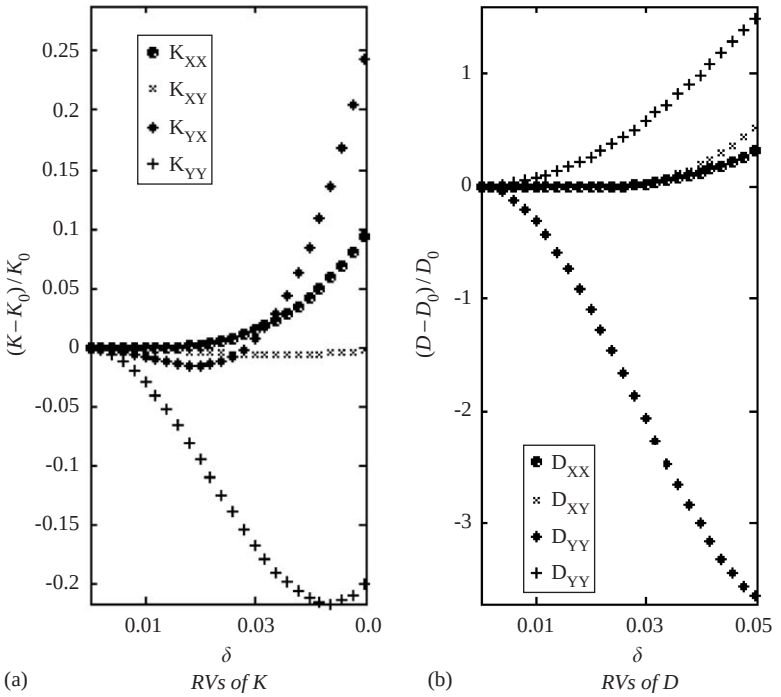

Fig. 11. Relative variations of linear coefficients of bearing vs. dimensionless excitation amplitude δ ($F_Y = 1.3$).

It can be observed from Fig. 11(a) ($F_Y = 1.3$), at ($\delta = 0.05$, the RVs of stiffness coefficients exceed 10% (except for K_{XY}); while in Fig. 10(a) ($F_Y = 0.35$), at $\delta = 0.1$, the RVs are not over 10% (except for K_{XY}). A similar trend occurs in damping coefficients. When $F_Y = 1.3$ (in Fig. 11(b)), at $\delta = 0.05$, all RVs of damping coefficients exceed 30%; while at $F_Y = 0.35$ (in Fig. 10(b)), $\delta = 0.05$, none of the RVs exceeds over 30%. Both of the observations indicate that the coefficients are more sensitive to the excitation amplitude in the case of large load parameters than in the case of small load parameters.

Analyzing these figures, more observations can be found. Under the same condition, each coefficient's RV has different sensitivity to excitation amplitude. K_{XY} and D_{YX} are most sensitive among the eight coefficients. It indicates that the linear coefficients are sensitive to the excitation amplitude, and the sensitivity is varied for different coefficients. In the case of large load parameters, the influence of excitation amplitude on the identified coefficients becomes larger. Therefore, linear oil-film coefficients should be identified using small amplitude excitation so as to ensure them reliable.

The above observations have revealed the nonlinear characters of oil-film forces. In the case of small amplitude excitation, the oil-film forces can be simplified as linear models. The experimental results prove that the linear model is valid under this condition. However, when the excitation amplitude becomes large, the nonlinear characters of the oil-film forces cannot be ignored. If the linear model were still used to describe the oil-film forces, the coefficients would change greatly. Therefore, the linear model is invalid and a new nonlinear model should be reconstructed in this case.

4. Conclusions

The following conclusions can be drawn from the above experimental study:

1. The least-mean-square method in time domain is a fast and effective algorithm to identify the linear coefficients of journal bearings. The identified coefficients are repeatable and stable under conditions of small load parameter.
2. The experiments show that linear coefficients increase with the growth of the load parameter. This is in agreement with the theoretical calculation.
3. Because the velocity is acquired through a FIR differential filter, there is some noise involved. It results in larger degree of scatter occurring in the identified damping coefficients than in the identified stiffness coefficients.
4. The linear oil-film dynamic coefficients are sensitive to the excitation amplitude. Under the same operation condition, the influence of excitation amplitude on the identified coefficient is varied for different coefficients.
5. In the case of small load parameter, the identified dynamic coefficients are repeatable and stable. While in the case of large load parameter, the influence of excitation amplitude on the identified coefficients becomes larger, so the identified coefficients scatter to some extent. In this case, small amplitude excitation should be employed to receive reliable coefficients.
6. Under conditions of the large excitation amplitude, because nonlinear components in the oil-film forces are no longer negligible errors, the conventional linear model is invalid and nonlinear oil-film force models should be adopted.

Acknowledgements

The supports from the National Natural Science Foundation of China (Grant No. 90210007 and 50335030) and China 863 High Tech Project (2002AA412410) are gratefully acknowledged.

Appendix A. The differentiator

In order to achieve the velocity and the acceleration from the measured displacement, a differentiator (an FIR filter) is employed. Its principle is as follows.

It is assumed that $y(t)$ is the derivative of $x(t)$ with respect to time t

$$y(t) = \mathrm{d}x(t)/\mathrm{d}t. \tag{A.1}$$

Make Laplace transformation to Eq. (A.1), it turns into:

$$Y(s) = sX(s). \tag{A.2}$$

Substitute $s = \mathrm{j}\omega$ into Eq. (A.2), the transfer function can be gained

$$Y(\omega)/X(\omega) = \mathrm{j}\omega. \tag{A.3}$$

In other words, the derivative of $x(t)$ can be received by filtering it with a specific filter whose transfer function is $H(\omega) = \mathrm{j}\omega$. In this work, a FIR filter is chosen, and its order

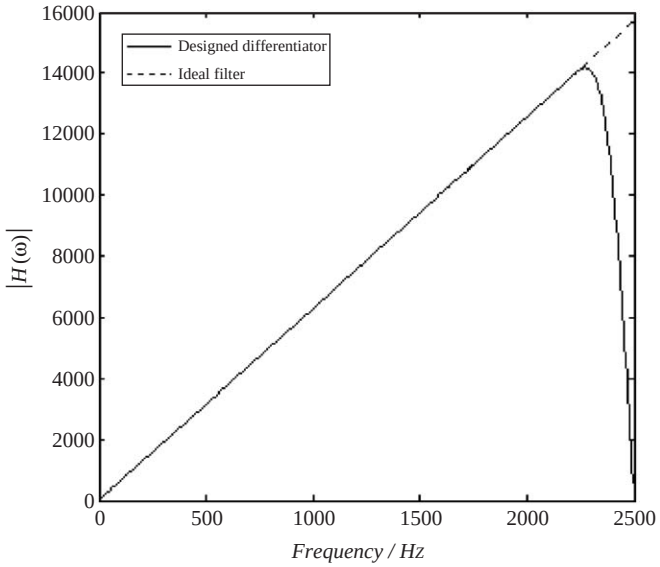

Fig. 12. Comparison between the designed filter and the ideal filter.

$n = 40$, its sampling frequency $f_s = 5000$ Hz. Fig. 12 depicts the filter's transfer function, and the ideal transfer function has also been shown in this figure. From this figure, it can be observed that the filter will fail to work once the displacement signal has components over 2000 Hz. In fact, the displacement data has been filtered through a low-pass filter before this process. The designed differentiator can satisfy the application demand in this work.

Due to the differentiator's slope-shaped transfer function, the filter may magnify the high frequency noise involved in displacement signals. Though a low-pass filter has been used for the displacement signals, there exists more noise in velocity signals than in displacement signals.

References

[1] Z.L. Qiu, A.K. Tieu, Identification of sixteen dynamic coefficients of two journal bearings from impulse responses, *Wear* 212 (1997) 206–212.

[2] Y.Y. Zhang, Y.B. Xie, D.M. Qiu, Identification of linearized oil-film coefficients in a flexible rotor-bearing system, part I: model and simulation, *Journal of Sound and Vibration* 152 (1992) 531–547.

[3] Y.Y. Zhang, Y.B. Xie, D.M. Qiu, Identification of linearized oil-film coefficients in a flexible rotor-bearing system, part II: experiment, *Journal of Sound and Vibration* 152 (1992) 549–559.

[4] G. D Jiang, H. Hu, W. Xu, Z.W. Jin, Y.B. Xie, Identification of oil film coefficients of large journal bearings on a full scale journal bearing test rig, *Tribology International* 30 (1997) 789–793.

[5] A.K. Tieu, Z.L. Qiu, Identification of sixteen dynamic coefficients of two journal bearings from experimental unbalance responses, *Wear* 177 (1994) 63–69.

[6] G.J. Kostrzewsky, R.D. Flack, Accuracy evaluation of experimentally derived dynamic coefficients of fluid film bearings part I: development of method, *Tribology Transactions* 33 (1990) 105–114.

[7] G.J. Kostrzewsky, R.D. Flack, Accuracy evaluation of experimentally derived dynamic coefficients of fluid film bearings part II: case studies, *Tribology Transactions* 33 (1990) 115–121.
[8] L.A. Branagan, Thermal Analysis of Fixed and Tilting Pad-Journal Bearings Including Cross-film Viscosity Variations and Deformations, PhD Dissertation, University of Virginia, Charlottesville, VA, 1988.
[9] Z.L. Qiu, A.K. Tieu, The effect of perturbation amplitudes on eight force coefficients of journal bearing, *Tribology Transactions* 39 (1996) 469–475.
[10] S.X. Zhao, A Study on Nonlinear Dynamic Properties of Journal Bearing, PhD Thesis, Xi'an Jiaotong University, China, 2003.